# Strain effects on the structural, magnetic, and thermodynamic properties of the Au(001)/Fe(001) interface from first principles

Magali Benoit, Nicolas Combe, Anne Ponchet, Joseph Morillo, Marie-José Casanove

# Strain effects on the structural, magnetic, and thermodynamic properties of the Au(001)/Fe(001) interface from first principles

Magali Benoit,[1] Nicolas Combe,[1,2] Anne Ponchet,[1] Joseph Morillo,[1,2] and Marie-José Casanove[1]
[1]*CEMES CNRS UPR8011, 29 rue Jeanne Marvig, 31055 Toulouse Cedex, France*
[2]*Université Paul Sabatier, 118 Route de Narbonne, 31062 Toulouse, France*
(Received 11 July 2014; revised manuscript received 8 September 2014; published 30 October 2014)

The structural, magnetic, and thermodynamic properties of the Au(001)/Fe(001) interface are investigated as a function of the in-plane strain using density functional theory calculations for two different Au slab thicknesses: 2 and 8 monolayers. The structural and magnetic properties are analyzed by studying the interlayer distance in the direction perpendicular to the interface and the atomic magnetic moments of Fe atoms, as a function of the in-plane strain. The structural study evidences both the bulk elastic and surface and interface contributions. The atomic magnetic moments of Fe atoms are essentially dependent on their local environment (number and distance of the Fe first neighbors). Thermodynamic properties of the interface are investigated through the calculation of the interface energy and interface stress. These thermodynamic quantities are subsequently used in a simple model to evaluate the strain state of an ideal spherical symmetric Fe@Au core-shell nanoparticle. The surface elastic effects are found to be significant for nanoparticles of diameter smaller than ∼20 nm and predominant for diameters smaller than ∼2.3 nm. Interface elastic effects are weaker than surface elastic effects but can not be neglected for very small nanoparticles ($\lesssim$1.9 nm) or for thin shells.

DOI: 10.1103/PhysRevB.90.165437 PACS number(s): 71.15.Mb, 68.35.bd, 68.35.Md, 61.46.Df

## I. INTRODUCTION

Targeted functionalization of nanoparticles is one of the current major challenges for applications as diverse as optics, catalysis, and biomedicine [1]. In particular, the combination of two types of metals and/or semiconductors together with the effects of the small size of the nanoparticles can significantly increase their potential functionalization [2–4].

The case of bimetallic nanoparticles is especially interesting since it combines the chemical order effects with the size effect. Depending on the two considered metals and on the growth conditions, different types of chemical order can occur (an alloy or a Janus, core-shell, or multishell arrangement) [5]. However, beyond the sole effect of the chemical order, the morphology of the nanoparticle can also affect its properties. Indeed, the presence or absence of well-defined crystalline facets on its surface can have a major impact on its properties, in particular on its catalytic reactivity or, for biomedical applications, on its ability to provide well-defined attachment sites for targeted molecules.

In the last decade, investigations were conducted in order to develop the synthesis of nanoparticles formed of well-faceted heterostructures, with the aim to obtain specific properties [3,4,6]. However, the emergence of a particular faceted morphology for a bimetallic nanoparticle is still very poorly understood. It depends on many factors which come into play, including the surface and interfacial energies, the elastic energies, the chemical potentials, etc.

In this work, we investigate the properties of the interface between a gold layer and an iron substrate, encountered in core-shell Fe@Au nanoparticles that were recently grown on a UHV magnetron sputtering setup [7,8]. Such nanoparticles are potentially interesting for applications since they combine some of the Fe and Au properties. The crystalline iron core shows a significant magnetization and magnetic anisotropy, while the well-defined crystalline facets of the biocompatible Au shell provide some well-controlled anchoring sites for targeted molecules.

A model of the synthesized Fe@Au nanoparticles was derived from the morphological and structural characteristics evidenced by transmission electron microscopy (TEM). The nanoparticles, 8–10 nm large, present a cubic bcc iron core and an epitaxied truncated fcc gold pyramid on each iron cube facet. A sketch of the model is displayed in Fig. 1.

Taking into account the epitaxial relationship at the gold/iron interface, i.e., Au(001)[100]//Fe(001)[110], the lattice mismatch $m_{\mathrm{Au/Fe}}$ defined as

$$m_{\mathrm{Au/Fe}} = (a_{\mathrm{Au}} - \sqrt{2}a_{\mathrm{Fe}})/\sqrt{2}a_{\mathrm{Fe}} \quad (1)$$

is equal to +0.66% with $a_{\mathrm{Au}} = 4.08$ Å [9] and $a_{\mathrm{Fe}} = 2.866$ Å [10] being the Au and Fe lattice parameters. As a consequence, regarding (volume) elastic energies, the Fe core is expected to be slightly in expansion while the gold shell is expected to be in compression. In the vicinity of the interface, one can make the assumption that the strain field is biaxial and can be decomposed into a parallel and a perpendicular component.

In addition to these (volume) elastic energies, due to the very small size (few nanometers) of the nanoparticles, the surface/interface effects, namely, the surface stress at the free nanoparticle surface and the interface stress at the Au/Fe interface, play a significant role in the strain field of the nanoparticle [11].

Experimental studies of surface and interface properties are difficult, so there is interest in computing these properties from atomistic simulations. Among them, the density functional theory (DFT) provides a relevant tool to the study of the structural, electronic, and magnetic properties of materials. Surface properties are provided by the DFT modeling of an infinite slab while interface properties can be obtained by the DFT modeling of two joined slabs, one of them playing the role of the substrate. Most of the theoretical works on metallic interfaces have considered an infinite, and

 

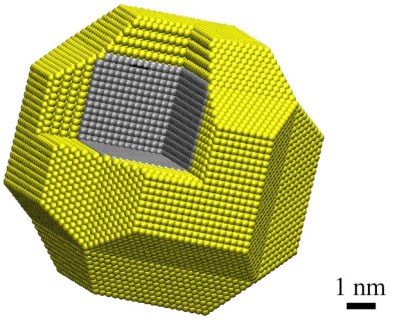


FIG. 1. (Color online) Sketch of the Fe@Au nanoparticle as deduced from high-resolution transmission electron microscopy (HRTEM) images. Fe and Au atoms are represented in gray and yellow, respectively. An eighth of the nanoparticle was removed to show the Fe core.

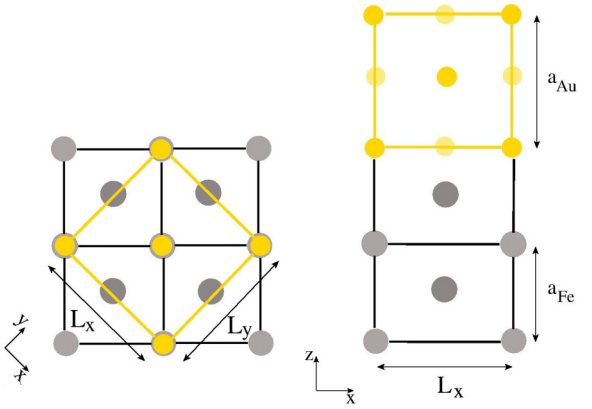


FIG. 2. (Color online) Sketch of the Au(001)/Fe(001) interface model. Gray and yellow disks are Fe and Au atoms, respectively. $L_x$ and $L_y$ indicate the simulation box sizes in the Au[100] and Au[010] directions (adapted from Ref. [8]).

thus unstrained, model substrate [8,12–16]. Accordingly, in a previous work [8], we have investigated, using DFT, the properties of the (001)Au/(001)Fe interface as a function of the number of deposited Au layers for an infinite and unstrained Fe substrate.

However, given the size of the observed Fe@Au nanoparticles [7] and following the above arguments, the Fe cube is not unstrained and its elastic state results from the contribution of surface and interface energies and of volume elastic energies.

In this paper, we investigate the effects of the Au shell on the Fe core by calculating the Au/Fe interface properties varying the in-plane interface strain state from the Fe unstrained state (0% of in-plane strain in Fe) to the Au unstrained state (0% of in-plane strain in Au). Sections II and III, respectively, report the simulations methods and the results of our study. Especially, in Secs. III A and III B, the structural and magnetic properties are analyzed in details as a function of the interface strain state. In Sec. III C, the interface stress and energy are extracted from the calculations. Finally, Sec. IV presents a simple model used to evaluate the effects of the surface and interface stresses on the strained state of the Fe@Au nanoparticle.

## II. SIMULATION DETAILS

In order to model the Au(001)/Fe(001) interface, a fcc crystalline slab of Au is placed on top of a crystalline bcc slab of Fe, with a rotation at 45° according to the epitaxial relationship found in the Fe@Au nanoparticle (see Fig. 2). Both crystals have the common crystalline [001] direction ($z$ axis) perpendicular to the free surfaces and the Au/Fe interface. The $x$ axis is defined along the [100] crystalline direction of Au corresponding to the $[1\bar{1}0]$ direction in Fe, while the $y$ axis, along the [010] of the Au crystal, corresponds to the [110] of the Fe crystal. The Fe slab is composed of $n_{\mathrm{Fe}} = 12$ atomic layers corresponding to a thickness of $e_{\mathrm{Fe}} \approx 17$ Å while two thicknesses $e_{\mathrm{Au}} \approx 17$ and 4 Å of the Au slab corresponding to $n_{\mathrm{Au}} = 8$ and 2 layers are investigated. Periodic boundary conditions are applied in all directions, with a vacuum of ≈12 Å in the [001] direction to separate the slabs from their periodic images. The simulation box sizes $L_x = L_y$ in the $x$ and $y$ directions are chosen so that the simulation box contains only one unit cell of the crystalline structure of both materials in these directions. The in-plane strain of the slabs is imposed by fixing the size of the simulation box in the $x$ and $y$ directions.

The interface system was simulated in the DFT framework using the VASP simulation package [17]. The simulations were performed using projector augmented-wave pseudopotentials with the $3d$ and $4s$ electrons as valence electrons for Fe and with the $5d$ and $6s$ electrons as valence electrons for Au. A cutoff energy of 600 eV ensures the convergence of the results with respect to the plane-wave basis set. A broadening, using the Methfessel and Paxton scheme of order 1 [18], was used with a smearing of 0.05 eV for the electron occupation. A $k$-point grid of $12\times12\times1$ was used following the Monkhosrt-Pack scheme and the Perdew-Burke-Ernzerhof (PBE) generalized gradient approximation (GGA) has been used for the exchange and correlation energy. The choice of this PBE exchange and correlation functional was thoroughly discussed in Ref. [8]. Using this functional, the surface and bulk characteristics of Fe compare well with experiments, whereas those of Au are less satisfactory. In particular, the Au lattice parameter and the (001) surface energy are, respectively, overestimated by +2.3% and underestimated by approximately −41.8%. The other tested exchange and correlation functionals (LDA, PBEsol [19], and the optBP86 together with a van der Waals dispersion [20]) improve the description of the bulk and surface properties of Au but deteriorate the ones of Fe. Since the investigated Fe@Au core-shell nanoparticles present a bigger iron core than the Au shell, the PBE functional, well suited for the modeling of iron, has been used throughout this study. A noticeable consequence of this choice is the overestimated value of the lattice mismatch $m_{\mathrm{Au/Fe}}$ [Eq. (1)] which is found to be +4.11% at the (001)Au/(001)Fe interface using DFT-PBE calculations, compared to the experimental value of $m_{\mathrm{expt}} = +0.66\%$. The error induced by this disagreement on surface and interface properties has been discussed in detail and estimated in Ref. [8].

In order to impose the in-plane strain of the slabs, the $L_x$ and $L_y$ sizes of the simulation box are changed from

$L_x = L_y = \sqrt{2}a_{\mathrm{Fe}} = 4.009$ Å to $L_x = L_y = a_{\mathrm{Au}} = 4.174$ Å, corresponding, respectively, to the Fe and Au equilibrium bulk lattice parameters obtained from DFT-PBE calculations. Four intermediate values of $L_x = L_y$ were investigated: 4.03, 4.06, 4.09, and 4.13 Å. The in-plane strain $\epsilon_{\parallel}^{\mathrm{Fe}}$ or $\epsilon_{\parallel}^{\mathrm{Au}}$ can be defined with respect to the unstrained Fe or Au bulk crystals. Both definitions are equivalent and describe the same physical system. These quantities and the relation linking them are

$$\epsilon_{\parallel}^{\mathrm{Fe}} = \epsilon_{xx}^{\mathrm{Fe}} = \epsilon_{yy}^{\mathrm{Fe}}, \tag{2}$$

$$\epsilon_{\parallel}^{\mathrm{Au}} = \epsilon_{xx}^{\mathrm{Au}} = \epsilon_{yy}^{\mathrm{Au}}, \tag{3}$$

$$\epsilon_{\parallel}^{\mathrm{Fe}} = \frac{a_{\mathrm{Au}}}{\sqrt{2}a_{\mathrm{Fe}}}\epsilon_{\parallel}^{\mathrm{Au}} + m_{\mathrm{Au/Fe}}, \tag{4}$$

where $m_{\mathrm{Au/Fe}}$ is the lattice mismatch [Eq. (1)], $\epsilon_{xx}^{\mathrm{R}}$ (resp. $\epsilon_{yy}^{\mathrm{R}}$) is the strain tensor component in the $xx$ (resp. $yy$) direction using the reference $\mathrm{R} \in \{\mathrm{Fe}, \mathrm{Au}\}$:

$$\epsilon_{\alpha\alpha}^{\mathrm{Fe}} = \frac{L_\alpha - \sqrt{2}a_{\mathrm{Fe}}}{\sqrt{2}a_{\mathrm{Fe}}} \quad \text{with} \quad \alpha \in \{x, y\}, \tag{5}$$

$$\epsilon_{\alpha\alpha}^{\mathrm{Au}} = \frac{L_\alpha - a_{\mathrm{Au}}}{a_{\mathrm{Au}}} \quad \text{with} \quad \alpha \in \{x, y\}. \tag{6}$$

In the following, we will also use the parameter $\rho$ which is defined as

$$\rho = \frac{\sqrt{2}a_{\mathrm{Fe}}}{a_{\mathrm{Au}}}, \tag{7}$$

thus

$$m_{\mathrm{Au/Fe}} = \rho^{-1} - 1, \tag{8}$$

$$\epsilon_{\parallel}^{\mathrm{Au}} = \rho(\epsilon_{\parallel}^{\mathrm{Fe}} + 1) - 1, \tag{9}$$

$$\epsilon_{\parallel}^{\mathrm{Fe}} = \rho^{-1}(\epsilon_{\parallel}^{\mathrm{Au}} + 1) - 1. \tag{10}$$

The selected $L_x = L_y$ values thus correspond to in-plane strain values of $\epsilon_{\parallel}^{\mathrm{Fe}}$ (resp. $\epsilon_{\parallel}^{\mathrm{Au}}$) equal to 0% (resp. −3.95%), +0.52% (resp. −3.45%), +1.27% (resp. −2.73%), +2.02% (resp. −2.01%), +3.02% (resp. −1.05%), and +4.11% (resp. 0%). For each $L_x = L_y$ value, a full optimization of the atomic positions has been performed.

Since the physical properties of the system can be described using both references, either Fe or Au bulk crystals, we have chosen to present the results as a function of the in-plane strain $\epsilon_{\parallel}^{\mathrm{Fe}}$ defined with respect to Fe, in the following.

## III. RESULTS AND DISCUSSION

### A. Structural properties

Figure 3 reports the evolution of the relative interlayer distances $\Delta d_i$ in the [001] direction as a function of the position $i$ in the slab and for the different in-plane strains $\epsilon_{\parallel}^{\mathrm{Fe}}$. Figures 3(a) and 3(b), respectively, report these data for the systems with 2 Au ML and 8 Au ML. For $i > 0$, $\Delta d_{-i}$ and $\Delta d_{+i}$, respectively, in the Fe and Au slabs, write as

$$\Delta d_{-i} = \frac{d_{i,i+1} - d_{\mathrm{Fe}}}{d_{\mathrm{Fe}}}, \tag{11}$$

$$\Delta d_{+i} = \frac{d_{i,i+1} - d_{\mathrm{Au}}}{d_{\mathrm{Au}}}, \tag{12}$$

where $d_{i,i+1}$ is the interlayer distance between the two consecutive $i$th and $i+1$th (001) atomic planes in the slab (the index of the layer in the slab being numbered starting from the interface) and $d_{\mathrm{Fe}}$ and $d_{\mathrm{Au}}$ are the corresponding values in the unstrained bulk material, i.e., $d_{\mathrm{Fe}} = a_{\mathrm{Fe}}/2$ and $d_{\mathrm{Au}} = a_{\mathrm{Au}}/2$. At the interface, the relative interlayer distance $\Delta d_0 = (d_0 - d_{\mathrm{FeAu}})/d_{\mathrm{FeAu}}$ is defined with respect to the average value $d_{\mathrm{FeAu}}$ between the Fe and the Au planes $d_{\mathrm{FeAu}} = (a_{\mathrm{Fe}} + a_{\mathrm{Au}})/4$, and $d_0$ is the interlayer distance between the Fe and Au (001) atomic planes at the interface.

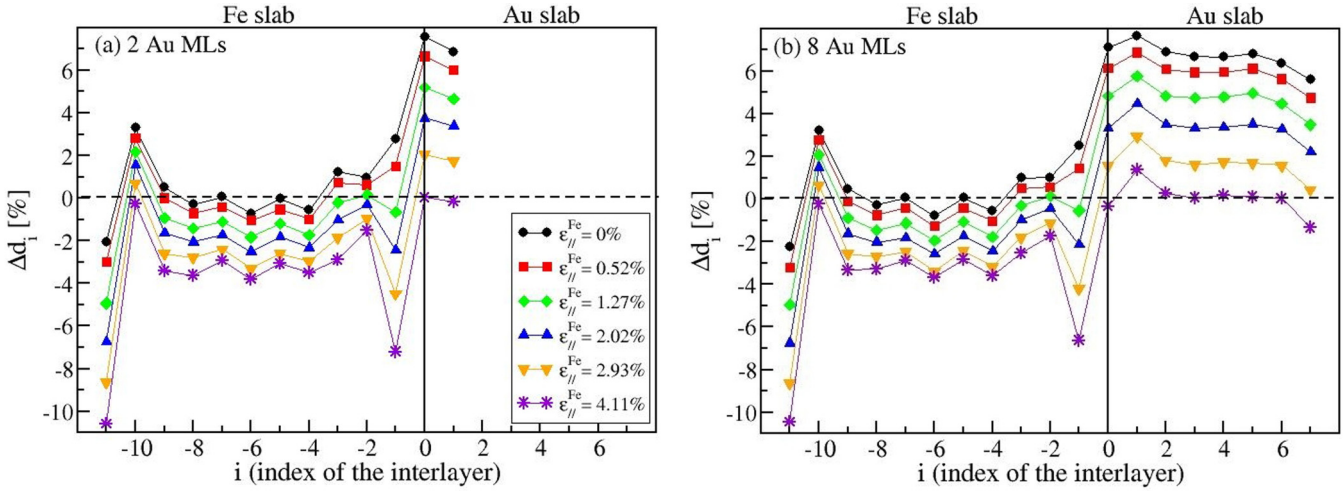


FIG. 3. (Color online) Relative interlayer distance in the Fe and Au slabs as a function of in-plane strains $\epsilon_{\parallel}^{\mathrm{Fe}}$: (a) for the system with 2 Au ML, (b) for the system with 8 Au ML. The index in the $x$ axis corresponds to the position of the interlayer numbered from the interface (see text).

The structural characteristics of the two systems, with 2 Au ML and with 8 Au ML, are very similar. We will first describe and discuss the results obtained for the 8 Au ML system.

For $\epsilon_{\parallel}^{Fe}= 0\%$ [black circles in Fig. 3(b)] in the 8 Au ML system, the Fe slab is not subject to any in-plane strain. The relative interlayer distances in Fe are close to the bulk one in the center of the slab and deviate from it at the free surface and at the interface. At the free Fe surface, the relative interlayer distance of the last couple of (001) planes is contracted ($\Delta d_{-11} \approx -2.0\%$), while the next one is expanded ($\Delta d_{-10} \approx +3.5\%$). Inside the Au slab, the relative interlayer distance converges to a value of $\approx$+6.8% in the center of the Au slab. This latter value can relevantly be compared to the expectation value $\epsilon_{\perp}^{Au}$ given by the linear elasticity theory: The out-of-plane strain can be expressed as a function of the in-plane strain and of the $C_{11}^{Au}$ and $C_{12}^{Au}$ Au elastic constants in cubic crystals following:

$$[\epsilon_{\perp}^{Au}]_{elast} = -\frac{2C_{12}^{Au}}{C_{11}^{Au}}\epsilon_{\parallel}^{Au} \tag{13}$$

yielding $[\epsilon_{\perp}^{Au}]_{elast} = +5.4\%$. The discrepancy between our results and this prediction is mainly attributed to the failure of the linear elasticity theory to accurately describe highly strained (larger than 1% or 2%) systems. Indeed, by computing $\epsilon_{\perp}^{Au}$ as a function of $\epsilon_{\parallel}^{Au}$ in the Au bulk, we found that deviations from the linearity occur around 1%. For $\epsilon_{\parallel}^{Au} = -3.95\%$ (i.e., $\epsilon_{\parallel}^{Fe} = 0\%$), $\epsilon_{\perp}^{Au}$ in the bulk is $\approx +6.7\%$, close to the value $\approx$+6.8% reported in Fig. 3(b) inside the Au slab. The remaining difference between the bulk value $\epsilon_{\perp}^{Au} = +6.7\%$ and the reported one is attributed to the limited thickness of the Au slab. At the free Au surface, the Au relative interlayer distance $\Delta d_7 \approx +5.6\%$ is slightly contracted with respect to the one in the center of the slab. In the vicinity of the interface, expansions of the Fe and Au relative interlayer distances are observed $\Delta d_{-1} \approx +2.5\%$ and $\Delta d_1 \approx +7.1\%$. These results concerning the relative interlayer distances for $\epsilon_{\parallel}^{Fe}= 0\%$ are consistent with our previous results [8].

For $\epsilon_{\parallel}^{Fe} = +4.11\%$, or equivalently for an unstrained Au slab $\epsilon_{\parallel}^{Au} = 0\%$, the Fe relative interlayer distance converges to a value of $\Delta d \approx -3.5\%$ in the center of the Fe slab. The prediction of the linear elasticity theory is

$$[\epsilon_{\perp}^{Fe}]_{elast} = -\frac{2C_{12}^{Fe}}{C_{11}^{Fe}}\epsilon_{\parallel}^{Fe} \tag{14}$$

yielding $[\epsilon_{\perp}^{Fe}]_{elast} = -4.4\%$. Again, the discrepancy between our results and this prediction is attributed to nonlinear elastic effects and to the limited thickness of the slab. Computing $\epsilon_{\perp}^{Fe}$ for $\epsilon_{\parallel}^{Fe} = +4.11\%$ in the Fe bulk, we find $\epsilon_{\perp}^{Fe} = -3.6\%$ in close agreement with the reported value in Fig. 3(b). At the free Fe surface, the system behaves similarly to the case of the unstrained Fe slab, but this behavior is here enhanced: The relative interlayer distance between the last couple of (001)Fe planes is very strongly contracted $\Delta d_{-11} = -10.5\%$, while the next one $\Delta d_{-10} = -0.2\%$ almost corresponds the Fe bulk value. Inside the Au slab, the interlayer distance in the center of the Au slab is, as expected, very close from the unstrained bulk one. At the free surface of the Au slab, and similarly to the observation done in the case of a strained Au slab [8], a contraction is observed $\Delta d_7 \approx -1.3\%$. This contraction only concerns the two (001) planes of the Au slab close to the surface. In the vicinity of the interface, the relative interlayer distance $\Delta d_1 \approx +1.4\%$ is significantly larger than in the center of the slab: This phenomenon, already observed in the case of a strained Au slab, is more pronounced here. Beneath the interface, the Fe relative interlayer distance $\Delta d_{-1} \approx -6.6\%$ is strongly contracted while the next one $\Delta d_{-2} \approx -1.7\%$ is significantly larger than the one in the center of the Fe slab. For values of $\epsilon_{\parallel}^{Fe}$ between 0% and +4.11%, a monotonous evolution of the relative interlayer distances in both the Fe and the Au slabs is observed. This monotonous evolution is, however, different for the interlayer distances inside the slabs, and for the ones at the surface (or interface).

In order to investigate the surface and interface effects on the relative interlayer distances as a function of the in-plane strain independently on the bulk elastic properties, we define the corrected relative interlayer distance $\delta^{cor}d_i$ as the difference of the relative interlayer distances and the relative interlayer distances in the bulk material:

$$\delta^{cor}d_i = \Delta d_i - \Delta^{bulk}d_i,$$

where $\Delta^{bulk}d_i$ is the bulk relative interlayer distance in Au and Fe for positive and negative values of $i$. For $i = 0$, $\Delta^{bulk}d_0$ is defined as the average value between the Au and Fe bulk relative interlayer distances. The resulting values $\delta^{cor}d_i$ thus report the perpendicular excess strain at the free Fe and Au surfaces and at the Au/Fe interface, due to the in-plane strain. Such excess strain can be related to the *surface strain* [11].

Figure 4 reports the corrected relative interlayer distances for different in-plane strains. Inside the Au and Fe slabs, for all the in-plane strains, the corrected relative interlayer distance $\delta^{cor}d_i$ almost cancels: The small remaining excess of perpendicular excess strain is attributed to the finite thickness of the Au and Fe slabs. More interestingly, at the surface and interface of the Fe slab, a strong excess of perpendicular strain

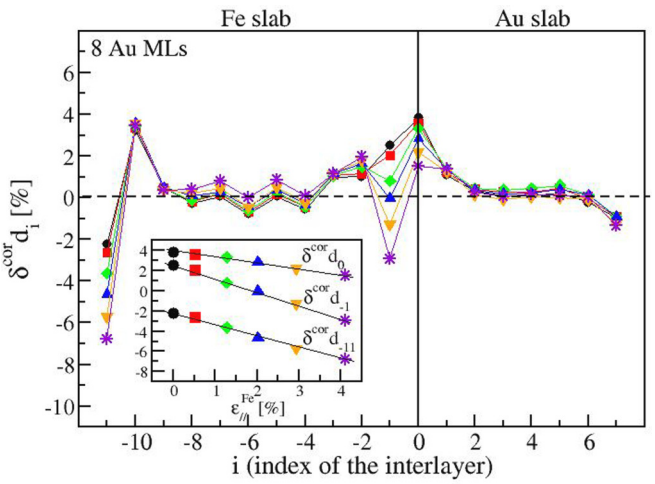


FIG. 4. (Color online) Corrected relative interlayer distance in the Fe and Au slabs as a function of in-plane strains $\epsilon_{\parallel}^{Fe}$ for the system with 8 Au ML. The index in the $x$ axis corresponds to the position of the interlayer numbered from the interface. Inset: Evolution of $\delta^{cor}d_{-11}$, $\delta^{cor}d_{-1}$, and $\delta^{cor}d_0$ as a function of the in-plane strain $\epsilon_{\parallel}^{Fe}$.

dependent on the in-plane strain is observed: The inset of Fig. 4 reports $\delta^{cor}d_{-1}$ and $\delta^{cor}d_{-11}$ as a function of $\epsilon_{\parallel}^{Fe}$. $\delta^{cor}d_{-1}$ and $\delta^{cor}d_{-11}$ are linearly dependent on the in-plane strain, with a very similar slope. On the contrary, the excess of perpendicular strain at the surface and interface of the Au slab, characterized by $\delta^{cor}d_7$ and $\delta^{cor}d_1$, are roughly independent on the in-plane strain. Finally, the corrected relative interlayer distance $\delta^{cor}d_0$ related to the Fe-Au distances decreases with the in-plane strain following a linear relation, with a coefficient smaller than $\delta^{cor}d_{-1}$ and $\delta^{cor}d_{-11}$ (inset of Fig. 4).

Let us now discuss the relative interlayer distances for the 2 Au ML system reported Fig. 3(a). They behave in a similar way than the ones presented in Fig. 3(b) for the system with 8 Au ML. However, the interlayer distances at the interface, i.e., $\Delta d_0$, are slightly larger in the 2 Au ML system than in the 8 Au ML system, whatever the in-plane strain. The Au slab is thus closer to the Fe interface layer when more Au layers are deposited. This result will be discussed in the light of the results obtained on the interface energy and on the charge-transfer calculations, which are presented in Sec. III C.

Finally, it is worth noticing that, for all the investigated in-plane strain values, the relative interlayer distance at the free Au surface $\Delta d_1$ is different in the 2 Au ML system with respect to the one in the 8 Au ML system, due to the proximity between the Au surface and the interface.

### B. Magnetic properties

Figure 5 reports the atomic magnetic moment of the Fe atoms as a function of their positions in the slab for different in-plane strain values in the systems with 8 and with 2 Au ML.

For the two Au slab thicknesses, the Fe atomic magnetic moment follows a similar evolution as a function of the atomic positions. For $\epsilon_{\parallel}^{Fe} = 0\%$, focusing on the 8 Au ML system, the Fe magnetic moment converges to a value of 2.17 $\mu_B$/at., very close to its bulk value (2.2 $\mu_B$/at.) in the center of the Fe slab. At the free Fe surface, the atomic magnetic moment is strongly enhanced reaching a value of 2.94 $\mu_B$/at.. Near the interface, the atomic magnetic moment is also enhanced, although the enhancement is slightly smaller, yielding 2.77 $\mu_B$/at.. Both enhancements of the atomic magnetic moment near the free surface and the Au/Fe interface are a consequence of the reduced number of Fe neighbors for these atoms.

For $\epsilon_{\parallel}^{Fe} = +4.11\%$, the Fe magnetic moment significantly increases inside the Fe slab reaching a value of 2.39 $\mu_B$/at.. The modification of the atomic magnetic moment as a function of the strain field has already been studied in magnetic materials [21] and in particular in Fe [22]. In the Fe slab, the net result of the increase of the in-plane strain $\epsilon_{\parallel}^{Fe}$ and of the simultaneous decrease of the out-of-plane strain $\epsilon_{\perp}^{Fe}$ (see Sec. III A) is a global increase of the average first-neighbor Fe-Fe distance from $\bar{d}_{Fe\text{-}Fe} \approx 2.45$ Å (for $\epsilon_{\parallel}^{Fe} = 0\%$) to $\bar{d}_{Fe\text{-}Fe} \approx 2.50$ Å (for $\epsilon_{\parallel}^{Fe} = +4.11\%$). This induces a change of the orbital hybridization and yields an increase of the atomic magnetic moment inside the slab from 2.17 $\mu_B$/at to 2.39 $\mu_B$/at.

At the free Fe surface and at the Au/Fe interface, whatever the in-plane strain and the number of Au planes, the atomic magnetic moments are enhanced reaching approximately the values of 2.94 and 2.77 $\mu_B$/at. Taking into account both the out-of-plane and in-plane strains, the average first-neighbor Fe-Fe distance $\bar{d}_{Fe\text{-}Fe}$ barely changes with the in-plane strain in the vicinity of the surface or interface. It varies from $\bar{d}_{Fe\text{-}Fe} \approx 2.43$ Å (for $\epsilon_{\parallel}^{Fe} = 0\%$) to $\bar{d}_{Fe\text{-}Fe} \approx 2.44$ Å (for $\epsilon_{\parallel}^{Fe} = +4.11\%$) in the close vicinity of the surface, and between $\bar{d}_{Fe\text{-}Fe} \approx 2.48$ Å (for $\epsilon_{\parallel}^{Fe} = 0\%$) and $\bar{d}_{Fe\text{-}Fe} \approx 2.47$ Å (for $\epsilon_{\parallel}^{Fe} = +4.11\%$) in the close vicinity of the interface. The atomic magnetic moments of the Fe atoms at the interface and at the surface are hence barely affected by the in-plane strain.

For values of $\epsilon_{\parallel}^{Fe}$ between 0% and +4.11%, a monotonous evolution of the atomic magnetic moments as a function of the atomic positions is observed between the two extreme cases detailed above.

Finally, a small magnetic moment of ≈0.06 $\mu_B$/at. is found on the Au atoms in the vicinity of the interface. however, this value scarcely changes with the number of Au planes, or with the in-plane strain.

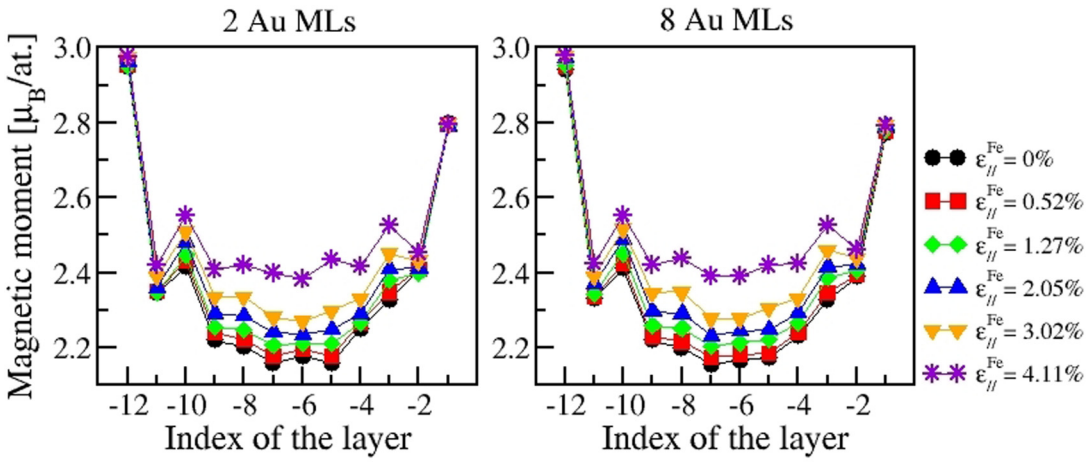


FIG. 5. (Color online) Evolution of the atomic magnetic moment of the Fe atoms as a function of the position of the layer in the Fe(001) slab, for the different values of in-plane strains $\epsilon_{\parallel}^{Fe}$ in the system with 8 Au ML (left) and 2 Au ML (right).

### C. Thermodynamic properties

In this section, the interface thermodynamic properties are investigated, modeled using the surface/interface elasticity theory and correlated to the electronic properties.

The energy difference $\Delta E(L_x,L_y)$ required to reversibly separate an interface into two free surfaces is studied as a function of the cell sizes $L_x$ and $L_y$ which are related to the in-plane strains $\epsilon_{\parallel}^{\mathrm{Fe}}$ and $\epsilon_{\parallel}^{\mathrm{Au}}$ [Eqs. (2) and (3)]. This energy difference is related to the work of adhesion $W_{\mathrm{ad}}$ through $W_{\mathrm{ad}} = \Delta E(L_x,L_y)/A$, $A$ being the interface area. $\Delta E(L_x,L_y)$ can be estimated using

$$\Delta E(L_x,L_y) = E_{(001)\mathrm{Au}}(L_x,L_y) + E_{(001)\mathrm{Fe}}(L_x,L_y) - E_{\mathrm{Au/Fe}}(L_x,L_y). \quad (15)$$

$E_{\mathrm{Au/Fe}}(L_x,L_y)$ is the total energy of the (001)Au/(001)Fe system with the cell sizes $L_x$ and $L_y$, while $E_{(001)\mathrm{Au}}(L_x,L_y)$ and $E_{(001)\mathrm{Fe}}(L_x,L_y)$ are the total energies of the (001)Au and (001)Fe free slabs, with the same cell sizes and with the same number of Au and Fe atoms. The calculations of $E_{\mathrm{Au/Fe}}(L_x,L_y)$, $E_{(001)\mathrm{Au}}(L_x,L_y)$, and $E_{(001)\mathrm{Fe}}(L_x,L_y)$ are performed using the same DFT conditions (same cutoff energy and same number of $k$ points).

Figure 6 reports the energy difference $\Delta E(L_x,L_y)$ for the two (001)Au/Fe(001) systems, respectively, composed of 2 and 8 Au ML, that is depicted as a function of the in-plane strain $\epsilon_{\parallel}^{\mathrm{Fe}}$ [which is related to $L_x$ and $L_y$ through Eq. (2)] for simplicity.

The energy difference $\Delta E(L_x,L_y)$ increases linearly with the in-plane strain $\epsilon_{\parallel}^{\mathrm{Fe}}$. The bonding between Au and Fe is stronger when the system is subject to a positive in-plane strain $\epsilon_{\parallel}^{\mathrm{Fe}}$. Moreover, the energy difference is larger for the system with 2 Au ML than for the system with 8 ML, whatever the in-plane strain.

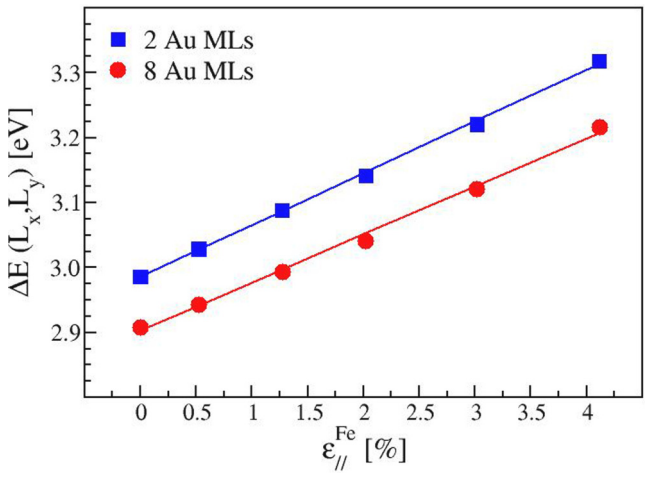


FIG. 6. (Color online) Energy difference $\Delta E(L_x,L_y)$ [Eq. (15)] as a function of the in-plane strain $\epsilon_{\parallel}^{\mathrm{Fe}}$ for the two systems, with 2 Au ML (blue squares) and with 8 Au ML (red circles) calculated using different simulation box sizes $L_x = L_y =$ 4.009, 4.03, 4.06, 4.09, 4.013, and 4.174 Å. The straight lines are linear fits.

TABLE I. Bader atomic charges (in $e$) of the Au and Fe atoms close to the interface, for the two extreme values of the in-plane strain and for the two systems with 8 Au ML and with 2 Au ML.

| | 2 Au ML | | 8 Au ML | |
|---|---|---|---|---|
| $\epsilon_{\parallel}^{\mathrm{Fe}}$ (%) | 0 | 4.11 | 0 | 4.11 |
| $\mathrm{Au}_{\mathrm{int+1}}$ | 11.058 | 11.063 | 11.022 | 11.023 |
| $\mathrm{Au}_{\mathrm{int}}$ | 11.240 | 11.264 | 11.269 | 11.296 |
| $\mathrm{Fe}_{\mathrm{int}}$ | 7.695 | 7.696 | 7.701 | 7.703 |
| $\mathrm{Fe}_{\mathrm{int-1}}$ | 8.002 | 7.998 | 8.013 | 7.998 |
| $\mathrm{Fe}_{\mathrm{int-2}}$ | 7.992 | 7.975 | 7.990 | 7.975 |

#### 1. Charge transfer

The larger bonding for the 2 Au ML system compared to the 8 ML system in the case of an unstrained Fe slab $\epsilon_{\parallel}^{\mathrm{Fe}} = 0\%$ has been previously related to the electronic properties of the interface and, more precisely, has been attributed to the very strong coupling between the orbitals of the Fe atoms at the interface and those of the Au atoms at the free surface [8]. The coupling between the orbitals of the Fe atoms and those of the Au atoms in the vicinity of the interface is related to the charge transfer, which can be evaluated by computing the atomic charges following the Bader approach [23]. For an unstrained Fe slab $\epsilon_{\parallel}^{\mathrm{Fe}} = 0\%$, we previously found that this coupling decreases with the distance between the Au atoms at the free Au surface and the Fe atoms in the vicinity of the interface as soon as more than 3 Au layers are deposited.

We here extend the study of the charge transfer to the general case of a strained Fe/Au system. Table I reports the atomic charges for the Fe and Au atoms close to the interface for the two extreme values of the in-plane strain $\epsilon_{\parallel}^{\mathrm{Fe}} = 0\%$ and $\epsilon_{\parallel}^{\mathrm{Fe}} = +4.11\%$. The charges computation only considers the valence electrons so that the Fe and Au atoms charges are, respectively, expected to be $8e$ and $11e$ in the bulk unstrained materials. $\mathrm{Fe}_{\mathrm{int}}$ (resp. $\mathrm{Au}_{\mathrm{int}}$) designates here the Fe (resp. Au) monolayer at the interface in contact with the Au (resp. Fe) atoms, $\mathrm{Fe}_{\mathrm{int-1}}$ (resp. $\mathrm{Au}_{\mathrm{int+1}}$) the monolayer beneath (resp. over) $\mathrm{Fe}_{\mathrm{int}}$ (resp. $\mathrm{Au}_{\mathrm{int}}$).

The analysis of the Bader charges clearly shows a charge transfer at the interface from the Fe atoms to the Au atoms, independently on the in-plane strain. This charge transfer mainly concerns the Fe and Au atoms in the close vicinity of the interface. In addition, this charge transfer is sensitive to the in-plane strain $\epsilon_{\parallel}^{\mathrm{Fe}}$ and more weakly sensitive to the number of Au ML.

For systems with 8 Au ML, the charge transfer on the first two Au layers close to the interface ($\mathrm{Au}_{\mathrm{int}}$ and $\mathrm{Au}_{\mathrm{int+1}}$) is equal to $+0.291e$ for $\epsilon_{\parallel}^{\mathrm{Fe}} = 0\%$ and to $+0.319e$ for $\epsilon_{\parallel}^{\mathrm{Fe}} = +4.11\%$. This charge transfer comes from Fe orbitals of atoms in the first Fe layers close to the interface ($\mathrm{Fe}_{\mathrm{int}}$ and $\mathrm{Fe}_{\mathrm{int-1}}$). The larger transfer observed when the Fe slab is subject to a positive in-plane strain ($\epsilon_{\parallel}^{\mathrm{Fe}} = +4.11\%$) is consistent with a larger energy difference $\Delta E$ (Fig. 6) and a smaller interface distance [Fig. 3(b)].

For systems with 2 Au ML deposited on the Fe slab, at a given $\epsilon_{\parallel}^{\mathrm{Fe}}$, the charge transfer is slightly more pronounced than for the 8 Au ML system. If these charge transfers are very

small (and in the limit of accuracy of the charge estimation using the Bader method), the repartition of this charge transfer on the first layers close to the interface significantly differs for the 2 and 8 ML system. Note also that small discrepancies are observed between the present atomic charges and those presented in Ref. [8] which suggests that these quantities are quite sensitive to the system size and to geometrical constraints (number of layers of each metal, number of fixed layers, etc.).

From this study of the Bader charges, one can conclude that the variation of the energy difference $\Delta E(L_x,L_y)$ as a function of the in-plane strain $\epsilon_{\parallel}^{\mathrm{Fe}}$ is accompanied by a modification of the charge transfer on the two first Au layers close to the interface, as if the system behaved as a rigid-band model in this specific situation.

### 2. *Interface energy and stress*

In this section, the interface thermodynamic properties are modeled using the surface/interface elasticity theory [11]. To this end, the $E_{(001)\mathrm{Au}}(L_x,L_y)$, $E_{(001)\mathrm{Fe}}(L_x,L_y)$ and $E_{\mathrm{Au/Fe}}(L_x,L_y)$ quantities involved in Eq. (15) are specified. Two descriptions, the Eulerian or the Lagrangian one, can be used to do so. In the first case, the area $A$ relates to the deformed interface $A = L_xL_y$, while in the second, the area $A$ relates to a reference state area $A_0$ for the interface. We have decided to work in the framework of the Lagrangian description for all the following calculations.

The energy $E_{(001)\mathrm{Au}}(L_x,L_y)$ of a homogeneous Au free slab writes as

$$E_{(001)\mathrm{Au}}(L_x,L_y) = N_{\mathrm{Au}}E_{\mathrm{bulk}}^{\mathrm{Au}} + 2\gamma_0^{\mathrm{Au}}\,A_0^{\mathrm{Au}} + u_{el}^{\mathrm{Au}}V_0^{\mathrm{Au}} + 4\,\sigma_0^{\mathrm{Au}}\,\epsilon_{\parallel}^{\mathrm{Au}}\,A_0^{\mathrm{Au}}, \quad (16)$$

where $N_{\mathrm{Au}}$ is the number of Au atoms in the slab, $E_{\mathrm{bulk}}^{\mathrm{Au}}$ is the Au bulk energy per atom, $V_0^{\mathrm{Au}}$ and $A_0^{\mathrm{Au}}$ are the volume and area of the Au reference slab, taken here as an unstrained Au slab ($\epsilon_{\parallel}^{\mathrm{Au}} = \epsilon_{\perp}^{\mathrm{Au}} = 0\%$). $\gamma_0^{\mathrm{Au}}$ is the surface energy per unit area of the Au reference slab and $\sigma_0^{\mathrm{Au}}$ is the surface stress.

The Au slab is homogeneously strained so that, in the frame of the linear elasticity theory, the elastic energy per unit volume can be expressed as a function of the in-plane strain:

$$u_{el}^{\mathrm{Au}} = \left[C_{11}^{\mathrm{Au}} + C_{12}^{\mathrm{Au}} - 2\frac{C_{12}^{\mathrm{Au}2}}{C_{11}^{\mathrm{Au}}}\right](\epsilon_{\parallel}^{\mathrm{Au}})^2, \quad (17)$$

$C_{12}^{\mathrm{Au}}$ and $C_{11}^{\mathrm{Au}}$ being the Au elastic constants. Similar expressions can be obtained for the strained Fe slab:

$$E_{(001)\mathrm{Fe}}(L_x,L_y) = N_{\mathrm{Fe}}E_{\mathrm{bulk}}^{\mathrm{Fe}} + 2\gamma_0^{\mathrm{Fe}}\,A_0^{\mathrm{Fe}} + u_{el}^{\mathrm{Fe}}V_0^{\mathrm{Fe}} + 4\,\sigma_0^{\mathrm{Fe}}\,\epsilon_{\parallel}^{\mathrm{Fe}}\,A_0^{\mathrm{Fe}} \quad (18)$$

and

$$u_{el}^{\mathrm{Fe}} = \left[C_{11}^{\mathrm{Fe}} + C_{12}^{\mathrm{Fe}} - 2\frac{C_{12}^{\mathrm{Fe}2}}{C_{11}^{\mathrm{Fe}}}\right](\epsilon_{\parallel}^{\mathrm{Fe}})^2 \quad (19)$$

in which the elastic constants, the bulk energy, and the elastic energy per unit volume refer to Fe. The reference slab for the Fe system corresponds to an unstrained Fe slab ($\epsilon_{\parallel}^{\mathrm{Fe}} = \epsilon_{\perp}^{\mathrm{Fe}} = 0\%$). Note that we have assumed for simplicity the validity of the linear elasticity theory for the Au and Fe bulk in Eqs. (17) and (19). However, since the bulk elastic energies terms will cancel in Eq. (21) from Eqs. (20), (16), and (18), Eq. (21) will remain reliable beyond the linear elasticity assumption for bulk materials.

Using similar definitions for the reference interface area $A_0^{\mathrm{Au/Fe}}$, the interface energy $\gamma_0^{\mathrm{Au/Fe}}$ and the interface stress $\sigma_0^{\mathrm{Au/Fe}}$, the total energy of the (001)Au/(001)Fe system reads as

$$\begin{aligned} E_{\mathrm{Au/Fe}}(L_x,L_y) &= N_{\mathrm{Au}}E_{\mathrm{bulk}}^{\mathrm{Au}} + N_{\mathrm{Fe}}E_{\mathrm{bulk}}^{\mathrm{Fe}} + u_{el}^{\mathrm{Au}}V_0^{\mathrm{Au}} + u_{el}^{\mathrm{Fe}}V_0^{\mathrm{Fe}} \\ &\quad + \left(\gamma_0^{\mathrm{Au}} + 2\sigma_0^{\mathrm{Au}}\epsilon_{\parallel}^{\mathrm{Au}}\right)A_0^{\mathrm{Au}} + \left(\gamma_0^{\mathrm{Fe}} + 2\sigma_0^{\mathrm{Fe}}\epsilon_{\parallel}^{\mathrm{Fe}}\right)A_0^{\mathrm{Fe}} \\ &\quad + \left(\gamma_0^{\mathrm{Au/Fe}} + 2\sigma_0^{\mathrm{Au/Fe}}\epsilon_{\parallel}^{\mathrm{Au/Fe}}\right)A_0^{\mathrm{Au/Fe}}, \end{aligned} \quad (20)$$

where $\epsilon_{\parallel}^{\mathrm{Au/Fe}}$ is the in-plane strain defined with respect to the interface reference state. So, combining Eqs. (16), (18), and (20), the expression of $\Delta E(L_x,L_y)$ finally reads as

$$\Delta E(L_x,L_y) = \left(\gamma_0^{\mathrm{Au}} + 2\sigma_0^{\mathrm{Au}}\epsilon_{\parallel}^{\mathrm{Au}}\right)A_0^{\mathrm{Au}} + \left(\gamma_0^{\mathrm{Fe}} + 2\sigma_0^{\mathrm{Fe}}\epsilon_{\parallel}^{\mathrm{Fe}}\right)A_0^{\mathrm{Fe}} - \left(\gamma_0^{\mathrm{Au/Fe}} + 2\sigma_0^{\mathrm{Au/Fe}}\epsilon_{\parallel}^{\mathrm{Au/Fe}}\right)A_0^{\mathrm{Au/Fe}}. \quad (21)$$

In Eq. (20), the unstrained Fe (resp. Au) slab has been taken as a reference for the Fe (resp. Au) part of the Au/Fe system. Since there is no natural choice for the interface reference state, two reference systems will be considered in the following: the unstrained Au slab and the unstrained Fe slab. Of course, these two descriptions using two different reference systems are fully equivalent and describe the same physical system.

In the following, to unambiguously define an interface quantity $B$ ($B \in \{\gamma_0^{\mathrm{Au/Fe}},\sigma_0^{\mathrm{Au/Fe}},\epsilon_{\parallel}^{\mathrm{Au/Fe}},A_0^{\mathrm{Au/Fe}}\}$), its reference state $x$ will be mentioned using a subscript $[B]_x$ with $x \in \{\mathrm{Au},\mathrm{Fe}\}$.

*Au reference*. Assuming that the reference state for the interface is the unstrained Au slab: $[A_0^{\mathrm{Au/Fe}}]_{\mathrm{Au}} = A_0^{\mathrm{Au}}$ and $[\epsilon_{\parallel}^{\mathrm{Au/Fe}}]_{\mathrm{Au}} = \epsilon_{\parallel}^{\mathrm{Au}}$. Using Eqs. (4), (7), and (10), Eq. (21) reads as

$$\Delta E(\epsilon_{\parallel}^{\mathrm{Au}}) = \left[\gamma_0^{\mathrm{Au}} + \rho^2\gamma_0^{\mathrm{Fe}} - \left[\gamma_0^{\mathrm{Au/Fe}}\right]_{\mathrm{Au}} + \rho(1-\rho)\sigma_0^{\mathrm{Fe}} + 2\left(\sigma_0^{\mathrm{Au}} + \rho\sigma_0^{\mathrm{Fe}} - \left[\sigma_0^{\mathrm{Au/Fe}}\right]_{\mathrm{Au}}\right)\epsilon_{\parallel}^{\mathrm{Au}}\right]A_0^{\mathrm{Au}}. \quad (22)$$

*Fe reference*. The reference state for the interface is the one corresponding to the unstrained Fe slab. Hence, $[A_0^{\mathrm{Au/Fe}}]_{\mathrm{Fe}} = A_0^{\mathrm{Fe}}$ and $[\epsilon_{\parallel}^{\mathrm{Au/Fe}}]_{\mathrm{Fe}} = \epsilon_{\parallel}^{\mathrm{Fe}}$. Equation (21) now reads as

$$\Delta E(\epsilon_{\parallel}^{\mathrm{Fe}}) = \left[\gamma_0^{\mathrm{Fe}} + \rho^{-2}\gamma_0^{\mathrm{Au}} - \left[\gamma_0^{\mathrm{Au/Fe}}\right]_{\mathrm{Fe}} + 2\rho^{-1}(1-\rho^{-1})\sigma_0^{\mathrm{Au}} + 2\left(\sigma_0^{\mathrm{Fe}} + \rho^{-1}\sigma_0^{\mathrm{Au}} - \left[\sigma_0^{\mathrm{Au/Fe}}\right]_{\mathrm{Fe}}\right)\epsilon_{\parallel}^{\mathrm{Fe}}\right]A_0^{\mathrm{Fe}}. \quad (23)$$

Note that Eqs. (22) and (23) are equivalent provided a change of the superscript Au by Fe and of $\rho$ by $\rho^{-1}$.

From a linear fitting of $\Delta E(L_x,L_y)$ as a function of $\epsilon_{\parallel}^{\mathrm{Fe}}$ in Fig. 6 and the use of Eq. (23), the interface energy $[\gamma_0^{\mathrm{Au/Fe}}]_{\mathrm{Fe}}$ and stress $[\sigma_0^{\mathrm{Au/Fe}}]_{\mathrm{Fe}}$ are extracted. Similarly, from the plot of $\Delta E(L_x,L_y)$ as a function of $\epsilon_{\parallel}^{\mathrm{Au}}$ (not shown) and the use of Eq. (22), we extract the quantities $[\gamma_0^{\mathrm{Au/Fe}}]_{\mathrm{Au}}$ and $[\sigma_0^{\mathrm{Au/Fe}}]_{\mathrm{Au}}$. Note that the determination of these interface quantities requires the knowledge of the (001)Au and (001)Fe surface energies and stresses. These quantities have been computed at the same level of theory (DFT-PBE, same cutoff energy, and same number of $k$ points) than in the Au/Fe

TABLE II. Interface energy and stress obtained using the Au or Fe references for the interface.

| | [mJ/m$^2$] | 8 Au ML | 2 Au ML |
|---|---|---|---|
| Reference Au | $[\gamma_0^{\mathrm{Au/Fe}}]_{\mathrm{Au}}$ | 310.7 | 213.6 |
| | $[\sigma_0^{\mathrm{Au/Fe}}]_{\mathrm{Au}}$ | −438.7 | −729.5 |
| Reference Fe | $[\gamma_0^{\mathrm{Au/Fe}}]_{\mathrm{Fe}}$ | 374.6 | 291.8 |
| | $[\sigma_0^{\mathrm{Au/Fe}}]_{\mathrm{Fe}}$ | −456.8 | −700.6 |

system. The surface energies of (001)Au and (001)Fe and the surface stress of (001)Au have been computed previously and are equal to 873, 2478, and 1836 mJ/m$^2$, respectively [8]. The surface stress of (001)Fe has been computed following the same protocol used for (001)Au in Ref. [8] and is equal to 1328 mJ/m$^2$.

Table II reports the interface thermodynamic properties using both Au or Fe reference states. As already suggested, the thermodynamics properties of the interface described using the Au and Fe reference states are related since they describe the same physical system. From Eqs. (22) and (23),

$$\left[\sigma_0^{\mathrm{Au/Fe}}\right]_{\mathrm{Fe}} = \rho^{-1}\left[\sigma_0^{\mathrm{Au/Fe}}\right]_{\mathrm{Au}},$$
$$\left[\gamma_0^{\mathrm{Au/Fe}}\right]_{\mathrm{Fe}} = \rho^{-2}\left(\left[\gamma_0^{\mathrm{Au/Fe}}\right]_{\mathrm{Au}} - 2(1-\rho)\left[\sigma_0^{\mathrm{Au/Fe}}\right]_{\mathrm{Au}}\right).$$

Note that in our previous study [8], we found a slightly different value 356 mJ/m$^2$ for the interface energy with the Fe reference $[\gamma_0^{\mathrm{Au/Fe}}]_{\mathrm{Fe}}$: The previous calculations were not performed in exactly the same conditions as the present ones (the thicknesses of the Fe and Au slabs were different and the atoms at the free surface of the Fe slab were fixed to the bulk positions). The procedure to measure the interface energy, and especially the limited size of the investigated system, can hence lead to non-negiligible variations of the resulting $\gamma_0^{\mathrm{Au/Fe}}$ and $\sigma_0^{\mathrm{Au/Fe}}$ ($\approx \pm 5\%$).

The interfacial energy $E_{\mathrm{int}}$ is defined in the following:

$$E_{\mathrm{int}} = \gamma^{\mathrm{Au/Fe}} A_0^{\mathrm{Au/Fe}} = \left(\gamma_0^{\mathrm{Au/Fe}} + 2\sigma_0^{\mathrm{Au/Fe}}\epsilon_{\parallel}^{\mathrm{Au/Fe}}\right)A_0^{\mathrm{Au/Fe}}. \quad (24)$$

The interfacial energy does not depend on the choice of the reference state (Au or Fe). The Au(001)/Fe(001) interface defined by $A_0^{\mathrm{Au/Fe}} = A_0^{\mathrm{Fe}} = 2a_{\mathrm{Fe}}^2$ with a in-plane strain $\epsilon_{\parallel}^{\mathrm{Fe}} = 0\%$ using the Fe reference state can equivalently be described using the Au reference state by $A_0^{\mathrm{Au/Fe}} = A_0^{\mathrm{Au}} = a_{\mathrm{Au}}^2$ with an in-plane strain $\epsilon_{\parallel}^{\mathrm{Au}} = -3.95$. Both descriptions yield the same interfacial energy: $E_{\mathrm{int}} = 376$ meV. The same interface subject to tensile in-plane strain ($\epsilon_{\parallel}^{\mathrm{Fe}} = +4.11\%$ and $A_0^{\mathrm{Au/Fe}} = A_0^{\mathrm{Fe}} = 2a_{\mathrm{Fe}}^2$ using the Fe reference) presents an interfacial energy of $E_{\mathrm{int}} = 338$ meV. These two interfacial energies agree fairly well with an estimation obtained following the approach of Ref. [24], giving a value of 0.5 mJ/m$^2$ [25]. Moreover, the interfacial energy is found to be lower when the Fe substrate is subject to a positive in-plane strain, and the Au slab is undeformed. This result agrees with the more important charge transfer that was found in this case (see Table I) and with the negative value of the interface stress: The presence of the interface tends to expand slightly the Fe/Au system in the [100] and [010] directions.

### D. Effect of the interface/surface stresses on the strain field of a nanoparticle

In this section, the effect of the surface and interface stresses on the strained state of a Fe@Au core-shell nanoparticle in vacuum is evaluated using a simple model. Our aim here is to establish an order of magnitude of the deformation induced by the surface and interface stresses in the nanoparticle as a function of the size of the nanoparticle and of the ratio between the Au and Fe volumes. In order to do this evaluation, we make the following crude approximations:

(1) The nanoparticle has a spherical symmetry: both Fe core and nanoparticle are spherical with the same center and $D_{\mathrm{Fe}}$ and $D_{\mathrm{NP}}$ ($D_{\mathrm{Fe}} < D_{\mathrm{NP}}$) are their respective diameters.

(2) The strain field is homogeneous in the Fe core and Au shell.

(3) The elastic energy of the nanoparticle is described in the framework of the linear elasticity theory.

(4) Thermodynamic surface and interface properties are independent of their crystalline orientation.

(5) At the Au/Fe interface, there is an epitaxial relationship of the type Au(001)/Fe(001) as if the interface was planar.

(6) Surfaces or interface energies and stresses are independent of the Au shell thickness and are described by those of the planar Au(001) free surface and by the planar Au(001)/Fe(001) interfaces.

Within these approximations, the total energy $E_{\mathrm{NP}}(\epsilon_{\parallel}^{\mathrm{Fe}})$ of a Fe@Au nanoparticle as a function of the in-plane strain writes as

$$\begin{aligned} E_{\mathrm{NP}}(\epsilon_{\parallel}) = {} & N_{\mathrm{Au}}E_{\mathrm{bulk}}^{\mathrm{Au}} + N_{\mathrm{Fe}}E_{\mathrm{bulk}}^{\mathrm{Fe}} \\ & + u_{el}^{\mathrm{Au}}V_0^{\mathrm{Au}} + u_{el}^{\mathrm{Fe}}V_0^{\mathrm{Fe}} + \left(\gamma_0^{\mathrm{Au}} + 2\sigma_0^{\mathrm{Au}}\epsilon_{\parallel}^{\mathrm{Au}}\right)A_0^{\mathrm{Au}} \\ & + \left(\left[\gamma_0^{\mathrm{Au/Fe}}\right]_{\mathrm{Fe}} + 2\left[\sigma_0^{\mathrm{Au/Fe}}\right]_{\mathrm{Fe}}\epsilon_{\parallel}^{\mathrm{Fe}}\right)\left[A_0^{\mathrm{Au/Fe}}\right]_{\mathrm{Fe}}, \end{aligned} \quad (25)$$

where the Fe reference was chosen for the interface. $V_0^{\mathrm{Au}}$ and $A_0^{\mathrm{Au}}$ refer to the volume and free-surface area of the unstrained Au shell. $V_0^{\mathrm{Fe}}$ and $[A_0^{\mathrm{Au/Fe}}]_{\mathrm{Fe}}$ refer to the unstrained Fe core volume and to the Au/Fe interface area. Here, since we assume an epitaxial relationship of the type Au(001)/Fe(001) at the Au/Fe interface as if it was planar, the meaning of other quantities, defined previously for a slab, transposes straightforwardly to the case of the nanoparticle.

In Appendix, the total energy $E_{\mathrm{NP}}(\epsilon_{\parallel})$ of the nanoparticle is specified. The in-plane Fe strain $\epsilon_{\parallel}^{\mathrm{Fe}}$ that minimizes this energy is given by

$$\begin{aligned} \epsilon_{\parallel}^{\mathrm{Fe}} = {} & \left[\rho(1-\rho)C_{\mathrm{el}}^{\mathrm{Au}}(\beta^3-1) - \frac{6\beta^3}{D_{\mathrm{NP}}}\sigma_0^{\mathrm{Au}}\rho \right. \\ & \left. - \frac{6\beta}{D_{\mathrm{NP}}}\left[\sigma_0^{\mathrm{Au/Fe}}\right]_{\mathrm{Fe}}\right] \Big/ \left[\rho^2 C_{\mathrm{el}}^{\mathrm{Au}}(\beta^3-1) + C_{\mathrm{el}}^{\mathrm{Fe}}\right], \end{aligned} \quad (26)$$

where the following quantities were defined:

$$C_{\mathrm{el}}^{\mathrm{Au}} = C_{11}^{\mathrm{Au}} + C_{12}^{\mathrm{Au}} - 2\frac{C_{12}^{\mathrm{Au}\,2}}{C_{11}^{\mathrm{Au}}},$$
$$C_{\mathrm{el}}^{\mathrm{Fe}} = C_{11}^{\mathrm{Fe}} + C_{12}^{\mathrm{Fe}} - 2\frac{C_{12}^{\mathrm{Fe}\,2}}{C_{11}^{\mathrm{Fe}}}, \quad (27)$$
$$\beta = \frac{D_{\mathrm{NP}}}{D_{\mathrm{Fe}}}.$$

This strain $\epsilon_{\parallel}^{Fe}$ [Eq. (26)] gives an order of magnitude of the deformation induced by the surface and interface stresses in a Fe@Au nanoparticle as a function of its characteristics. The first term of the right-hand side of Eq. (26), referred as $[\epsilon_{\parallel}^{Fe}]_{bulk}$ in the following, originates from the lattice mismatch between Fe and Au and arises from the bulk elastic energies. The two next terms, respectively referred as $[\epsilon_{\parallel}^{Fe}]_{surf}$ and $[\epsilon_{\parallel}^{Fe}]_{inter}$, originate from the nanoparticle surface and from the Au/Fe interface. The values of the surface $\sigma_0^{Au}$ and interface $[\sigma_0^{Au/Fe}]_{Fe}$ stresses evaluated previously for a slab are used in Eq. (26).

Following this simple model, we are not only able to calculate the in-plane strain in the Fe core but also the relative importance of the volume, surface, and interface effects on the equilibrium state of the Fe@Au nanoparticle. We first fix the diameter of the Fe core to a value of $D_{Fe} = 1$ nm and compute the in-plane Fe strain calculated following Eq. (26). Figure 7(a) reports the values of $\epsilon_{\parallel}^{Fe}$ (solid lines) and $[\epsilon_{\parallel}^{Fe}]_{bulk}$(dashed line) as a function of the diameter $D_{NP}$ of the Fe@Au nanoparticle. The diameter $D_{NP}$ is varied from 1.5 to 40 nm. The in-plane Fe strain $\epsilon_{\parallel}^{Fe}$ is an increasing function of the nanoparticle diameter. Eluding the surface and interface effects, the Au shell tries to impose its lattice parameter to the Fe core yielding a Fe core in tension in agreement with the positive value of $[\epsilon_{\parallel}^{Fe}]_{bulk}$ regardless the nanoparticle size. Nevertheless, below a diameter of $D_{NP} \approx 2.3$ nm, the Fe core is found in compression ($\epsilon_{\parallel}^{Fe} < 0$) in Fig. 7(a) which underlines some surface or interface effects. The surface or interface effects compress the nanoparticle analogously to the pressure increase inside a soap bubble (Laplace law): such effect has already been experimentally and theoretically observed in metallic nanoparticles [26,27].

The surface and interface effects are directly related to the difference between $\epsilon_{\parallel}^{Fe}$ and $[\epsilon_{\parallel}^{Fe}]_{bulk}$. In order to precisely evaluate the relative weight of the surface and interface effects on the in-plane Fe strain, Fig. 7(b) reports the surface to bulk $\lambda$ and interface to bulk $\mu$ contribution ratios:

$$\lambda = \frac{[\epsilon_{\parallel}^{Fe}]_{surf}}{[\epsilon_{\parallel}^{Fe}]_{bulk}}, \tag{28}$$

$$\mu = \frac{[\epsilon_{\parallel}^{Fe}]_{inter}}{[\epsilon_{\parallel}^{Fe}]_{bulk}}. \tag{29}$$

Surface stress effects are found to be significant as soon as the nanoparticle diameter is smaller than 20 nm: $|\lambda| > 0.1$ for $D_{NP} < 20$ nm. They become comparable to the elastic bulk ones for nanoparticles with a diameter of 2.3 nm ($\lambda = -1$ for $D_{NP} = 2.3$ nm) and predominant below this diameter.

In turn, interface stress effects have a small contribution on the in-plane Fe strain compared to the surface ones except for small nanoparticles. The interface stress effects contribution represent less than 5% of the surface effects contribution ($|\frac{\mu}{\lambda}| < 0.05$) for $D_{NP} > 2.3$ nm. However, these interface effects become significant for very small nanoparticles and are no longer negligible ($\mu > 0.1$ for $D_{NP} < 1.9$ nm).

The effects of the Fe to Au volume ratio for a nanoparticle of fixed diameter are now investigated. Figure 8(a) reports the in-plane Fe strain $\epsilon_{\parallel}^{Fe}$ (solid lines) and its bulk contribution $[\epsilon_{\parallel}^{Fe}]_{bulk}$ (dashed line) as a function of the core diameter $D_{Fe}$ for a nanoparticle with fixed diameter $D_{NP} = 8$ nm, corresponding to the size of recently synthesized Fe@Au nanoparticles [7].

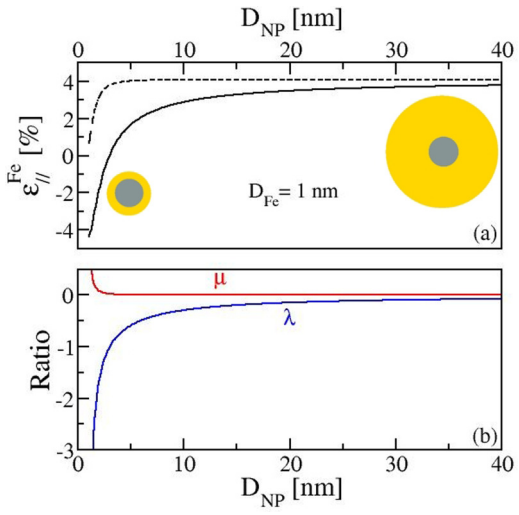


FIG. 7. (Color online) (a) In-plane Fe strain $\epsilon_{\parallel}^{Fe}$ (bold line) and its bulk contribution $[\epsilon_{\parallel}^{Fe}]_{bulk}$ (dashed line) in the Fe core for a fixed Fe core diameter $D_{Fe} = 1$ nm, as a function of the Fe@Au nanoparticle diameter $D_{NP}$ (solid line). The gray and yellow disks represent schematically the Fe core and Au shell relative sizes in the Fe@Au nanoparticle. (b) Relative contributions of the surface $\lambda$ and interface $\mu$ to the in-plane Fe strain in the Fe core compared to the bulk contribution as a function of the nanoparticle diameter.

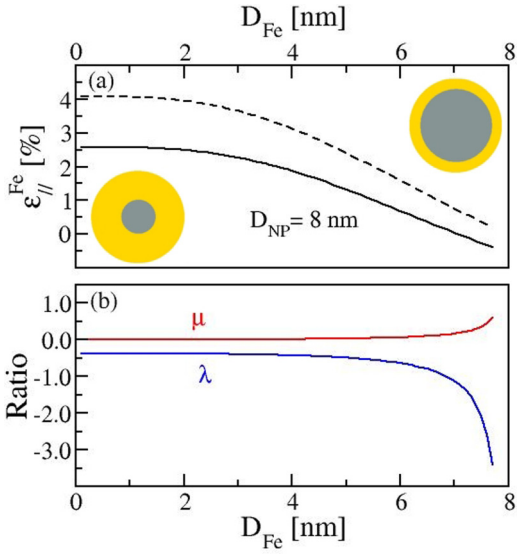


FIG. 8. (Color online) (a) In-plane Fe strain $\epsilon_{\parallel}^{Fe}$ (bold line) and its bulk contribution $[\epsilon_{\parallel}^{Fe}]_{bulk}$ (dashed line) in the Fe core as a function of the core diameter $D_{Fe}$ in a Fe@Au nanoparticle with a fixed diameter $D_{NP} = 8$ nm. The gray and yellow disks represent schematically the Fe core and Au shell relative sizes in the Fe@Au nanoparticle. (b) Relative contributions of the surface $\lambda$ (blue line) and interface $\mu$ (red line) to the in-plane Fe strain in the Fe core compared to the bulk contribution as a function of the nanoparticle diameter.

The diameter $D_{Fe}$ is varied from ∼0 to 7.6 nm. The in-plane strain is a decreasing function of the core diameter $D_{Fe}$. Eluding the surface and interface effects, the Fe to Au volume ratio increases with the core diameter $D_{Fe}$ and thus the elastic bulk effects of the Au shell decrease in agreement with the decrease of $[\epsilon_{\parallel}^{Fe}]_{bulk}$.

In Fig. 8(b), the relative contributions of the surface $\lambda$ and interface $\mu$ effects to the in-plane Fe strain, compared to the bulk contribution, are shown as a function of the Fe core diameter. The surface contribution is significant $|\lambda| > 0.25$ for all investigated core diameters. This result agrees with the above conclusion: Surface stress effects are significant as soon as the nanoparticle diameter is smaller than 20 nm. Moreover, the surface effects contribution increases (in absolute value) with the Fe core diameter in agreement with the decrease of the Au shell volume with $D_{Fe}$, while the Au surface $A_{Au}$ is independent of $D_{Fe}$.

Finally, the interface effects contribution $\mu$ compared to bulk ones increases with $D_{Fe}$. Indeed, the Au to Fe volume ratio and thus the bulk contribution decrease with $D_{Fe}$ while the Fe interface area $[A_0^{Au/Fe}]_{Fe}$ increases. The contribution of interface effects, although always smaller than the surface one, represents more than 5% of the surface contribution for $D_{Fe} > 4$ nm and should therefore not be neglected in a rigorous calculation.

As already mentioned, this model is very simplified and suffers from several assumptions. First, for a nanoparticle with $D_{NP} \approx 2$ nm and $D_{Fe} = 1$ nm in Fig. 7 or $D_{NP} \approx 8$ nm and $D_{Fe} = 7$ nm in Fig. 8, the Au shell typically corresponds to about 2 ML so that the approximations of the present simple model (spherical core and shell, surface and interface energies and stresses independent on the Au layer thickness and on the surface orientation) become more questionable. Especially, we previously showed that surface and interface energies and stresses are not independent on the Au shell thickness below a 3 Au ML [8]. Nevertheless, we believe that the correction induced by these physical ingredients would not significantly alter the surface and interface effects contribution to the in-plane Fe strain.

Second, the evolution of the Fe in-plane strain was computed with numerical values for the mismatch of +3.95% between Au(001) and Fe(001) extracted from DFT-PBE calculations which overestimates by a factor 6 the experimental one 0.66%. Comparing the surface to bulk $\lambda_{expt}$ and interface to bulk $\mu_{expt}$ contribution ratios using the experimental lattice parameters, and assuming all other calculated quantities (surface and interface energies and stresses) accurate, we find that

$$\lambda_{expt}/\lambda_{PBE} = \frac{1-\rho^{PBE}}{1-\rho^{expt}},$$

$$\mu_{expt}/\mu_{PBE} = \frac{\rho^{PBE}(1-\rho^{PBE})}{\rho^{expt}(1-\rho^{exp})},$$

where $\rho^{PBE} = \rho = 0.960\,41$ and $\rho^{expt} = 0.993\,42$. A subscript PBE has been added here to all the DFT calculations quantities. We find that $\lambda_{expt}/\lambda_{PBE} \approx 6.0$ and $\mu_{expt}/\mu_{PBE} \approx 5.8$ whatever the nanoparticle diameter. Hence, within these assumptions, the surface and interface effects are expected to be even more important than the above calculated ones. Note that if we have assumed that the calculated surface and interface stresses are comparable to the experimental ones, even an error of ≈50% on the surface and interface stresses would not change this conclusion.

Finally, we made the crude approximation of a homogeneous strain in the nanoparticle and that both the spherical core and the nanoparticle have the same center. However, an inhomogeneous strain or an asymmetrization of the core position would presumably relax the core stress by decreasing the bulk elastic energy [28] of both the Fe and Au systems while, in the mean time, surface and interface energies would not be drastically modified. A consequence of an asymmetric core position would thus be an increase of the surface $\lambda$ and interface $\mu$ effects to the in-plane Fe strain.

As a net result of this discussion on the regardless physical ingredients of our crude model, we conclude that the relative contributions of the surface $\lambda$ and interface $\mu$ is certainly underestimated in our simple model.

## IV. CONCLUSION

Using first-principles calculations based on DFT, we have investigated the structural, magnetic, and thermodynamic properties of the Au(001)/Fe(001) interface subject to an in-plane strain for two Au slab thicknesses: 2 and 8 ML. The structural properties and especially the perpendicular strain in the system through the relative interlayer distance have been investigated. Our calculations show that the interlayer distance at the interface Au(001)/Fe(001) decreases with the in-plane strain, suggesting a tendency for (001)Au to bind more strongly to (001)Fe when the Fe slab is in tension. The atomic magnetic moments of Fe atoms at the surface and at the interface, due to the reduced numbers of Fe first neighbors are enhanced compared to bulk ones and are found to be independent on the in-plane strain. Inside the Fe slab, the atomic magnetic moments of the Fe atoms increase with the in-plane strain in agreement with the increase of the average first-neighbor Fe-Fe distance. Finally, the interface energy and stress characterizing the thermodynamic properties of the interface have been calculated and subsequently used in a simple model developed in order to evaluate the strain state of an ideal spherical Fe@Au core-shell nanoparticle. The surface elastic effects are found to be significant for nanoparticles of diameter smaller than ∼20 nm and predominant for diameters smaller than ∼2.3 nm. Interface elastic effects are weaker than surface elastic effects but can not be neglected for very small nanoparticles ($\lesssim$1.9 nm) or for thin shells. Nevertheless, this model is very simple and omits several significant physical ingredients, which effects need to be evaluated by further calculations. Aside from the cited ones, the effect of a matrix or a liquid surrounding the nanoparticle has not been considered and would ask the determination of the elastic properties of the interface between the shell and this surrounding medium.

Finally, if these conclusions are dependent of the specific properties of the metals investigated in this study, they show that the interface and surface elastic effects can not be neglected when studying small core-shell nanoparticles, and that they can even become the predominant effects compared to elastic volume effects.

## ACKNOWLEDGMENTS

The authors thank H. Tang and N. Tarrat for fruitful discussions. Calculations have been performed on the CALMIP computer center (Project No. p1141) and on the CINES computer center (Projects No. c2013097067 and No. c20140907067).


## APPENDIX

In this appendix, the total energy of the spherical core-shell nanoparticle in the simple model is specified in the Fe reference and is then minimized with respect to the Fe strain state $\epsilon_{\parallel}^{\mathrm{Fe}}$.

Using Eqs. (17) and (19),

$$\begin{aligned} E_{\mathrm{NP}}(\epsilon_{\parallel}) = {} & N_{\mathrm{Au}} E_{\mathrm{bulk}}^{\mathrm{Au}} + N_{\mathrm{Fe}} E_{\mathrm{bulk}}^{\mathrm{Fe}} \\ & + \left[ C_{11}^{\mathrm{Au}} + C_{12}^{\mathrm{Au}} - 2\frac{C_{12}^{\mathrm{Au}\,2}}{C_{11}^{\mathrm{Au}}} \right] (\epsilon_{\parallel}^{\mathrm{Au}})^2 V_0^{\mathrm{Au}} \\ & + \left[ C_{11}^{\mathrm{Fe}} + C_{12}^{\mathrm{Fe}} - 2\frac{C_{12}^{\mathrm{Fe}\,2}}{C_{11}^{\mathrm{Fe}}} \right] (\epsilon_{\parallel}^{\mathrm{Fe}})^2 V_0^{\mathrm{Fe}} \\ & + \left( \gamma_0^{\mathrm{Au}} + 2\sigma_0^{\mathrm{Au}} \epsilon_{\parallel}^{\mathrm{Au}} \right) A_0^{\mathrm{Au}} \\ & + \left( \left[ \gamma_0^{\mathrm{Au/Fe}} \right]_{\mathrm{Fe}} + 2\left[ \sigma_0^{\mathrm{Au/Fe}} \right]_{\mathrm{Fe}} \epsilon_{\parallel}^{\mathrm{Fe}} \right) \left[ A_0^{\mathrm{Au/Fe}} \right]_{\mathrm{Fe}}. \end{aligned} \tag{A1}$$

$E_{\mathrm{NP}}(\epsilon_{\parallel})$ can be expressed as a function of $\epsilon_{\parallel}^{\mathrm{Fe}}$ only using the relation between $\epsilon_{\parallel}^{\mathrm{Au}}$ and $\epsilon_{\parallel}^{\mathrm{Fe}}$ [Eq. (4)]:

$$\begin{aligned} E_{\mathrm{NP}}(\epsilon_{\parallel}^{\mathrm{Fe}}) = {} & N_{\mathrm{Au}} E_{\mathrm{bulk}}^{\mathrm{Au}} + N_{\mathrm{Fe}} E_{\mathrm{bulk}}^{\mathrm{Fe}} + \gamma_0^{\mathrm{Au}} A_0^{\mathrm{Au}} \\ & + \left[ \gamma_0^{\mathrm{Au/Fe}} \right]_{\mathrm{Fe}} \left[ A_0^{\mathrm{Au/Fe}} \right]_{\mathrm{Fe}} + 2(\rho - 1)\sigma_0^{\mathrm{Au}} A_0^{\mathrm{Au}} \\ & + (\rho - 1)^2 C_{\mathrm{el}}^{\mathrm{Au}} V_0^{\mathrm{Au}} \\ & + 2\{ \rho(\rho - 1) C_{\mathrm{el}}^{\mathrm{Au}} V_0^{\mathrm{Au}} + \rho\sigma_0^{\mathrm{Au}} A_0^{\mathrm{Au}} \\ & + \left[ \sigma_0^{\mathrm{Au/Fe}} \right]_{\mathrm{Fe}} \left[ A_0^{\mathrm{Au/Fe}} \right]_{\mathrm{Fe}} \} \epsilon_{\parallel}^{\mathrm{Fe}} \\ & + \left( \rho^2 C_{\mathrm{el}}^{\mathrm{Au}} V_0^{\mathrm{Au}} + C_{\mathrm{el}}^{\mathrm{Fe}} V_0^{\mathrm{Fe}} \right) \left( \epsilon_{\parallel}^{\mathrm{Fe}} \right)^2, \end{aligned} \tag{A2}$$

where

$$C_{\mathrm{el}}^{\mathrm{Au}} = C_{11}^{\mathrm{Au}} + C_{12}^{\mathrm{Au}} - 2\frac{C_{12}^{\mathrm{Au}\,2}}{C_{11}^{\mathrm{Au}}},$$

$$C_{\mathrm{el}}^{\mathrm{Fe}} = C_{11}^{\mathrm{Fe}} + C_{12}^{\mathrm{Fe}} - 2\frac{C_{12}^{\mathrm{Fe}\,2}}{C_{11}^{\mathrm{Fe}}}.$$

The equilibrium state of the nanoparticle requires that the strain state $\epsilon_{\parallel}^{\mathrm{Fe}}$ of the nanoparticle minimizes $E_{\mathrm{NP}}(\epsilon_{\parallel})$. So,

$$\begin{aligned} \frac{\partial E_{\mathrm{NP}}}{\partial \epsilon_{\parallel}^{\mathrm{Fe}}} = {} & 2\{ \left( \rho^2 C_{\mathrm{el}}^{\mathrm{Au}} V_0^{\mathrm{Au}} + C_{\mathrm{el}}^{\mathrm{Fe}} V_0^{\mathrm{Fe}} \right) \epsilon_{\parallel}^{\mathrm{Fe}} \\ & + \rho(\rho - 1) C_{\mathrm{el}}^{\mathrm{Au}} V_0^{\mathrm{Au}} + \rho\sigma_0^{\mathrm{Au}} A_0^{\mathrm{Au}} \\ & + \left[ \sigma_0^{\mathrm{Au/Fe}} \right]_{\mathrm{Fe}} \left[ A_0^{\mathrm{Au/Fe}} \right]_{\mathrm{Fe}} \} \\ = {} & 0, \end{aligned}$$

which gives an expression for $\epsilon_{\parallel}^{\mathrm{Fe}}$:

$$\begin{aligned} \epsilon_{\parallel}^{\mathrm{Fe}} = {} & \{ \rho(1 - \rho) C_{\mathrm{el}}^{\mathrm{Au}} V_0^{\mathrm{Au}} - \rho\sigma_0^{\mathrm{Au}} A_0^{\mathrm{Au}} \\ & - \left[ \sigma_0^{\mathrm{Au/Fe}} \right]_{\mathrm{Fe}} \left[ A_0^{\mathrm{Au/Fe}} \right]_{\mathrm{Fe}} \} / \left( \rho^2 C_{\mathrm{el}}^{\mathrm{Au}} V_0^{\mathrm{Au}} + C_{\mathrm{el}}^{\mathrm{Fe}} V_0^{\mathrm{Fe}} \right). \end{aligned} \tag{A3}$$

To go beyond this result, we specify approximate expressions of the volume of the Fe core, of the area of the Au/Fe interface, of the volume of the Au shell, and of the area of the nanoparticle surface:

$$V_{\mathrm{Fe}} = \frac{\pi}{6} D_{\mathrm{Fe}}^3,$$

$$\left[ A_0^{\mathrm{Au/Fe}} \right]_{\mathrm{Fe}} = \pi D_{\mathrm{Fe}}^2,$$

$$V_{\mathrm{Au}} = \frac{\pi}{6} \left[ D_{\mathrm{NP}}^3 - D_{\mathrm{Fe}}^3 \right],$$

$$A_{\mathrm{Au}} = \pi D_{\mathrm{NP}}^2.$$

Using these expressions and defining $\beta = \frac{D_{\mathrm{NP}}}{D_{\mathrm{Fe}}}$, Eq. (A3) yields Eq. (26).


[1] B. Mehdaoui, A. Meffre, M.-L. Lacroix, J. Carrey, S. Lachaize, M. Gougeon, M. Respaud, and B. Chaudret, J. Magn. Magn. Mater. **322**, L49 (2010).

[2] C.-W. Yang, K. Chanda, P.-H. Lin, Y.-N. Wang, C.-W. Liao, and M. H. Huang, J. Am. Chem. Soc. **133**, 19993 (2011).

[3] D. Wang, H. L. Xin, R. Hovden, H. Wang, Y. Yu, D. A. Muller, F. J. DiSalvo, and H. D. Abruña, Nat. Mater. **12**, 81 (2013).

[4] M. K. Debe, Nature (London) **486**, 43 (2012).

[5] R. G. Chaudhuri and S. Paria, Chem. Rev. **112**, 2373 (2012).

[6] C.-W. Yang *et al.*, J. Am. Chem. Soc. **133**, 19993 (2011).

[7] C. Langlois *et al.* (unpublished).

[8] M. Benoit, C. Langlois, N. Combe, H. Tang, and M.-J. Casanove, Phys. Rev. B **86**, 075460 (2012); **87**, 119905 (2013).

[9] C. Kittel, *Introduction to Solid State Physics*, 6th ed. (Wiley, New York, 1986).

[10] A. Dewaele, M. Torrent, P. Loubeyre, and M. Mezouar, Phys. Rev. B **78**, 104102 (2008).

[11] P. Müller and A. Saùl, Surf. Sci. Rep. **54**, 157 (2004).

[12] A. Arya and E. A. Carter, J. Chem. Phys. **118**, 8982 (2003).

[13] A. Schlapka, M. Lischka, A. Groß, U. Käsberger, and P. Jakob, Phys. Rev. Lett. **91**, 016101 (2003).

[14] D. F. Johnson, D. E. Jiang, and E. A. Carter, Surf. Sci. **601**, 699 (2007).

[15] A. Arya and E. A. Carter, Surf. Sci. **560**, 103 (2004).

[16] S. Lu, Q.-M. Hu, M. P. J. Punkkinen, B. Johansson, and L. Vitos, Phys. Rev. B **87**, 224104 (2013).

[17] J. Hafner, Acta Mater. **48**, 71 (2000).

[18] M. Methfessel and A. T. Paxton, Phys. Rev. B **40**, 3616 (1989).

[19] J. P. Perdew, A. Ruzsinszky, G. I. Csonka, O. A. Vydrov, G. E. Scuseria, L. A. Constantin, X. Zhou, and K. Burke, Phys. Rev. Lett. **100**, 136406 (2008).

[20] J. Klimes, D. R. Bowler, and A. Michaelides, Phys. Rev. B **83**, 195131 (2011).

[21] Y. Nahas, V. Repain, C. Chacon, Y. Girard, J. Lagoute, G. Rodary, J. Klein, S. Rousset, H. Bulou, and C. Goyhenex, Phys. Rev. Lett. **103**, 067202 (2009).
[22] T. Shimada, Y. Ishii, and T. Kitamura, Phys. Rev. B **81**, 134420 (2010).
[23] R. F. W. Bader, Chem. Rev. **91**, 893 (1991).
[24] A. R. Miedema and F. J. A. den Broeder, Z. Metallkunde **70**, 14 (1979).
[25] D. Amram, L. Klinger, and E. Rabkin, Acta Mater. **61**, 5130 (2013).
[26] H. J. Wasserman and J. S. Vermaak, Surf. Sci. **22**, 164 (1970).
[27] R. Meyer, L. J. Lewis, S. Prakash, and P. H. J Entel, Phys. Rev. B **68**, 104303 (2003).
[28] D. Bochicchio and R. Ferrando, Phys. Rev. B **87**, 165435 (2013).